

Removal of Chlortetracycline Chlorhydrate by Photo-Fenton Process: Experimental Study and ANN Modelling

N. Boucherit,^a S. Hanini,^a A. Ibri,^b M. Laidi,^{a,*} and M. Roubehie-Fissa^a

^a Biomaterials and Transport Phenomena Laboratory (LBMPT), Yahia Fares University, Médéa, Algeria

^b Materials and Environment Laboratory (LME), Faculty of Technology, Yahia Fares University, Médéa, Algeria

This work is licensed under a Creative Commons Attribution 4.0 International License



Abstract

The present work aimed to study the feasibility of photo-Fenton oxidation for the degradation of chlortetracycline chlorhydrate (CTC) in aqueous solutions, as well as the modelling of system behaviour by artificial neural networks. The removal performance of CTC oxidation by the Photo-Fenton process was studied under solar radiation. Different parameters were studied, such as pH (3 to 5), and initial concentrations of CTC (0.1 to 10 mg l⁻¹), hydrogen peroxide (1.701 to 190.478 mg l⁻¹), and ferrous ions (2.8 to 103.6 mg l⁻¹). Results showed that a high removal efficiency of 92 % was achieved at pH 3 under optimised conditions, such as 10 mg l⁻¹ of CTC, 127.552 mg l⁻¹ of H₂O₂, and 36.4 mg l⁻¹ of Fe²⁺. The transformation of CTC molecules was proved by UV-visible and HPLC analyses, which showed that almost no CTC molecules were remaining in the treated solution. A multi-layer perceptron artificial neural network has been developed to predict the experimental removal efficiency of CTC based on four dimensionless inputs: molecular weight, and initial concentrations of CTC, hydrogen peroxide and ferrous ions. The best network has been found with a high determination coefficient of 0.9960, and with a very acceptable root mean square error 0.0108. In addition, the global sensitivity analysis confirms that the most influential parameter for the CTC removal by photo-Fenton oxidation is the initial concentration of ferrous cations with a relative importance of 33 %.

Keywords

Artificial neural networks, multi-layer perceptron, chlortetracycline chlorhydrate, modelling, photo-oxidation

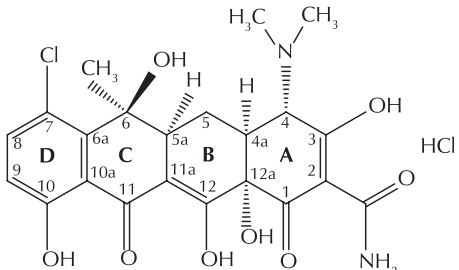
1 Introduction

Some pharmaceutical active ingredients are hazardous substances, because their presence in low amounts in the ecosystem and potential environmental impact have raised several issues in different natural matrices.^{1–3} Antibiotics are one of the largest groups of hazardous substances detected in the environmental samples that can cause a risk for all kinds of living organisms, including scenarios from ecological pollution to damage of biodiversity.^{4–6} Their presence even at trace levels can generate resistance in bacterial populations, and render antibiotics inefficient in the treatment of many infections.^{7,8} Moreover, the exposure of organisms to antibiotics for an extended time can lead to adverse effects, such as allergic or carcinogenic effects.⁷ Tetracyclines (TCs) are the second largest antibiotics used to treat human and animal infections due to their effective antimicrobial activity and minimal side effects.^{9,10} TCs are also used as feed additives for livestock and aquaculture. Thereby, they constitute approximately one-third of global antibiotic production and consumption.¹¹ Because of their stable chemical structure and low biodegradability, about 90 % of TCs are excreted non-transformed via the urine.^{9,10} This leads to their continuous entry into surface water, groundwater, drinking water and soil, and therefore, the food chain.^{10,12} Main sources of contamination by TCs are human and veterinary activities, the pharmaceutical industry and hospitals.¹³ Chlortetracycline chlorhydrate (CTC) is the first discovered molecule of the

TC family, and is the most frequently used for treatment in animal infections and as feed additive for animals.^{9,12,14} CTC is poorly absorbed (25–30 %) by living organisms, with maximum excretion ranging from 70 to 90 % in different environmental matrices.¹⁵ Hence, amounts of CTC have been found in surface water (122.3 ng l⁻¹) and wastewater (1.8 ± 0.5 mg l⁻¹).¹² While it has been reported by *Halling-Sørensen et al.*¹⁶ that the average half-life of CTC degradation ranges from 20 to 42 days in Danish agricultural soils, the natural degradation of the TC residue is still difficult. Incomplete mineralisation of CTC during Fenton oxidation and Fenton oxidation combined with ferro-sonication resulted in the formation of intermediate by-products which may pose risks to the environment.¹⁵ As the wastewater plants are the major source of the emerging microbial contaminants in the aqueous system, since they are unable to remove TCs efficiently, it has become inevitable to prevent/protect environmental matrices from this eventual contamination.¹² veterinary, and aquaculture applications. The continuous release of TCs residues into the environment and the inadequate removal through the conventional treatment systems result in its prevalent occurrence in soil, surface water, groundwater, and even in drinking water. As aqueous TCs contamination is the tip of the iceberg, and TCs possess good sorption capacity towards soil, sediments, sludge, and manure, it is insufficient to rely on the sorptive removal in the conventional water treatment plants. The severity of the TCs contamination is evident from the emergence of TCs resistance in a wide variety of microorganisms. This paper reviews the recent research on the TCs occurrence in the environmental matrices, fate in natural systems, toxic effects, and the

* Corresponding author: Maamar Laidi, PhD
Email: maamarw@yahoo.fr

Table 1 – Physicochemical properties of chlortetracycline chlorhydrate

Chemical structure	Characteristic	Value
	molecular weight/g mol ⁻¹	515.34
	solubility in water (at 293 K)/mg l ⁻¹	8.6
	density (at 293 K)/g ml ⁻¹	1.7±0.1
	appearance	yellow crystalline solid
	purity/%	98
	λ _{max} /nm	380
	pK _{a1} pK _{a2}	4.39 8.23

removal methods. The high performance liquid chromatography (HPLC) In this sense, studies on the presence and effects of these emerging contaminants, and on the processes of removing antibiotics, have been published.^{12,14} To reduce the ecological risk, many different methods have been tested for TC removal, such as adsorption/biosorption,^{9,10} chemical oxidation,^{1,12} ultra sonification-assisted catalase,¹⁷ micro-electrolysis,¹⁸ ion exchange,¹⁹ and membrane processes.²⁰ Advanced oxidation processes (AOPs) using photo-Fenton oxidation (PFO) are recognised as a promising technique for organic contaminant degradation or even mineralisation of organic pollutants. This technique is characterised by a simple process, fast reaction process rate, efficiency in non-selective degrading pollutants compounds and environmentally friendly solution for water treatment.^{15,21} AOPs are complex processes, since many parameters must be optimised simultaneously, which might be challenging if system modelling is done only by conventional methods. Recently, attention has focused on artificial neural networks (ANNs) due to their high-performance prediction and their inherent ability to simulate the different complex processes.²²⁻³⁰ ANN models work as black-box models and are developed only from experimental data.³¹ The objective of black-box modelling is to find, from available measurements of CTC removal, a deterministic relationship between the input variables of the model and the removal efficiency (RE). Nevertheless, only a limited number of studies on emerging microbial contaminants removal using ANN have been reported.^{25,32} Based on previous considerations, the present work aimed to investigate, for the first time, the removal of TC molecules such as chlortetracycline chlorhydrate (CTC) from aqueous solutions by advanced oxidation processes such as PF system. The effects of some operational parameters, such as aqueous phase pH, hydrogen peroxide, ferrous ions, and CTC concentrations were investigated to obtain the highest quantity and quality efficiency. Furthermore, the neural networks used in this study, the MLP-type supervised networks (multi-layer perceptron), were applied to predict the removal efficiency of CTC using the experimental results, and the performance of the established model was evaluated by the correlation coefficient (R^2) and the relative mean square error (RMSE).

2 Materials and methods

2.1 Materials

Chlortetracycline chlorhydrate (CTC), an antibiotic that is widely produced and used in Algeria, was chosen in this study. CTC was provided by the Antibiotical-Saidal pharmaceutical group (Medea, Algeria). The chemical structure and physicochemical properties are shown in Table 1. Hydrogen peroxide (30 %, v/v), hydrochloric acid (37 %), sodium hydroxide, buffer solutions (pH ranging from 3 to 5), and ferrous cations as ferrous sulphate, were purchased from Sigma-Aldrich Corporation (St. Louis, MO, USA).

2.2 Photo-Fenton treatment

Batch experiments were conducted in a borosilicate reactor (0.1 l). Experiments were conducted under the conditions cited in Table 2, they contained CTC, hydrogen peroxide, and ferrous ions for a reaction mixture of 50 ml. After 15 min, the reaction was immediately stopped by pH adjustment to 7. The effect of pH on removal efficiency was investigated by variation of pH values applying different buffers (pH 3 to 5). During the experiment, the solar radiation and luminescence ranged from 450 to 600 W m⁻² and 95 to 100 klx, respectively. The temperature in the reactor was maintained at 297.15±2.00 K using a water

Table 2 – Parameters and their values corresponding to their levels

Level N°	pH	[CTC] ₀ /mg l ⁻¹	[H ₂ O ₂] ₀ /mg l ⁻¹	[Fe ²⁺] ₀ /mg l ⁻¹
1	2.0	0.10	1.701	2.8
2	2.5	1.75	33.167	19.6
3	3.0	3.40	64.627	36.4
4	3.5	5.05	96.089	53.2
5	4.0	6.70	127.552	70.0
6	4.5	8.35	159.015	86.8
7	5.0	10.00	190.478	103.6

jacket. Finally, the mixture was centrifuged at 4000 rpm for 10 min. All experiments were carried out in duplicate and their average values were reported.

2.3 Analytical methods

CTC concentration was monitored by a UV-visible spectrophotometer (Perkin-Elmer 550 A, Wellesley, USA). Quantitative estimation of the residual CTC concentration after treatment with PFO was carried out on the supernatant at the maximum wavelength of CTC (380 nm). The removal efficiency (RE) was calculated as follows:

$$RE(\%) = \frac{C_0 - C_t}{C_0} \cdot 100 \quad (1)$$

where C_0 is initial CTC concentration (mg l^{-1}), and C_t is CTC concentration at time t (mg l^{-1}).

FTIR spectra of dried CTC and its precipitate metabolites were recorded for the KBr pellet. FTIR spectra were done using the absorbance mode in a Shimadzu 8400 spectrophotometer, Japan. An HPLC (Alliance Waters e2695) equipped with a UV-visible detector (Waters 2489) operated at 280 ± 4 nm, an automatic sample injector, a solvent delivery system, a thermostated column compartment adjusted at 318.15 K, and a reverse-phase column (RP8 with polar incorporated groups, $7.5 \text{ cm} \times 4.6 \text{ mm}$, $3.5 \mu\text{m}$, Sigma-Aldrich, USA) as a stationary phase used to acquire the elution of CTC and its extracted metabolites. The elution was conducted in a gradient program using a binary mobile phase gradient (Table 3), with a flow rate equal to 0.4 ml min^{-1} . The injection volume without the reduction agent was $100 \mu\text{l}$.

Table 3 – Mobile phase composition and program for the gradient method

Solvent	Distilled water	Perchloric acid	Dimethyl sulphoxide	Elution program /%, v/v
Mobile phase A	725 ml	50 ml	225 ml	100 → 0
Mobile phase B	250 ml	50 ml	700 ml	0 → 100

2.4 Artificial Neural Network

An artificial neural network (ANN) is a computational model used in artificial intelligence that is schematically inspired by biological neurons.³¹ In the present study, the input and output sets were obtained experimentally. The inputs consisting of four dimensionless variables, specifically molecular weights M_i^* , $[\text{CTC}]_0^*$, $[\text{H}_2\text{O}_2]_0^*$ and $[\text{Fe}^{2+}]_0^*$, were calculated by the Eqs. (2)–(5).

$$M_i^* = \frac{M_i}{701.262} \quad (2)$$

$$[\text{CTC}]_0^* = \frac{[\text{CTC}]_0}{\max([\text{CTC}]_0)} \quad (3)$$

$$[\text{H}_2\text{O}_2]_0^* = \frac{[\text{H}_2\text{O}_2]_0}{\max([\text{H}_2\text{O}_2]_0)} \quad (4)$$

$$[\text{Fe}^{2+}]_0^* = \frac{[\text{Fe}^{2+}]_0}{\max([\text{Fe}^{2+}]_0)} \quad (5)$$

M_i is the molecular weight of molecule i , and 701.262 is the total molecular weight of CTC, H_2O_2 and FeSO_4 . The corresponding removal efficiency (RE^*) was used as output.

Neural network training was performed using a MATLAB program (version R2018a). The data set was subdivided into training, testing, and validation sets, which contained 67, 17, and 16 % of the entire database, respectively. The normalisation of the input and the output was carried out using the function presented by Eq. (6).

$$y_{\text{norm}} = \frac{2(y - y_{\text{min}})}{(y_{\text{max}} - y_{\text{min}})} - 1 \quad (6)$$

where y_{norm} is the normalised value scaled between -1 and $+1$, y is the experimental data, while y_{max} and y_{min} are the maximum and the minimum experimental values, respectively. Since the RE is a static function that does not change over time, MLP was used for modelling tasks.³¹ The architecture of neural networks consisted of an input layer, a hidden layer with a tangent sigmoid transfer function (*tansig*), and an output layer with a linear function (*purelin*) (Fig. 1).

The best-adapted training algorithm, according to the literature,^{22,24,33} and after confirmation by an evaluative study, is the Levenberg-Marquardt (LM) algorithm. The accuracy of the developed ANN model was measured using R^2 ,

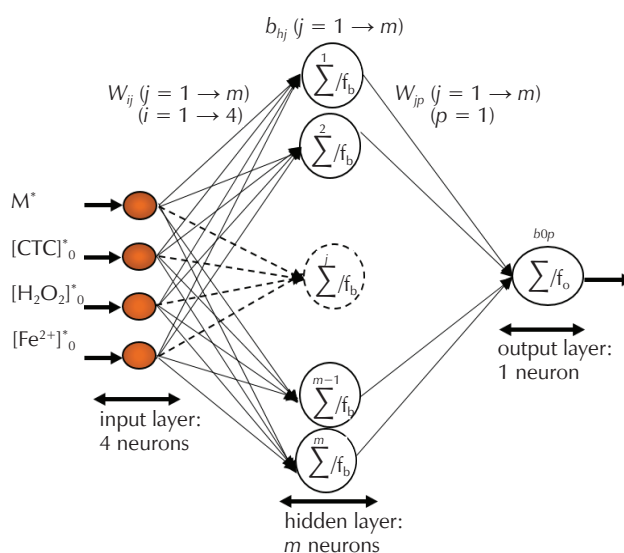


Fig. 1 – Architecture of the ANN

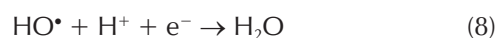
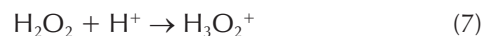
mean square error (MSE), root mean square error (RMSE), root of the normalised mean squared error (NRMSE), and absolute mean error (MAE).^{24,27,31} The determination of the best ANN architecture involves the selection of the optimal number of hidden neurons that is based on the minimum RMSE (close to 0) and highest R^2 (close to 1).³²

3 Results and discussion

3.1 Effect of pH, CTC, hydrogen peroxide and ferrous ions doses

In this part, the effect of pH, H_2O_2 , Fe^{2+} and CTC concentrations will be studied, and their optimisation rules will be outlined on the considerations existing in the literature. In all Fenton processes, pH is the key parameter in the transformation of organic molecules *in situ*, because it controls the concentration of ferrous ions, and consequently, the production of hydroxyl free radicals.³⁴⁻³⁶ As shown in Fig. 2, it is clear that the maximum removal of CTC reaches up to 82 % at pH 3. It has been reported that, when pH values are above 4, ferric cations formed and precipitated

onto various iron hydroxyls, leading to the production of sludge containing a high amount of Fe^{3+} . Also, in a strongly acidic medium ($pH < 2$), the reaction of hydrogen peroxide with ferrous ions could be slowed down because of the stability of H_2O_2 due to solvating a proton to form an oxonium ion (Eq. (7)).^{35,36} Moreover, the excess proton ions will react with the hydroxyl radical (Eq. (8)).³⁷



Therefore, according to Fig. 2, it is clear that the removal efficiency (RE) increased slowly with increasing the initial CTC concentration. The highest efficiency (82.21 %) was obtained for CTC concentrations of 10 mg l^{-1} . Hydrogen peroxide is a crucial parameter affecting the degradation efficiency of all organic pollutants. Therefore, it has been proved that oxidative transformation by PFO is improved with the increase in H_2O_2 dosage.^{35,36,38} Regarding Fig. 2, it was indicated that the removal of CTC molecules increased for H_2O_2 concentration ranging from 1.701 to $127.552 \text{ mg l}^{-1}$ and reached the maximum of 83.927 %. This dependence of H_2O_2 doses on molecule transforma-

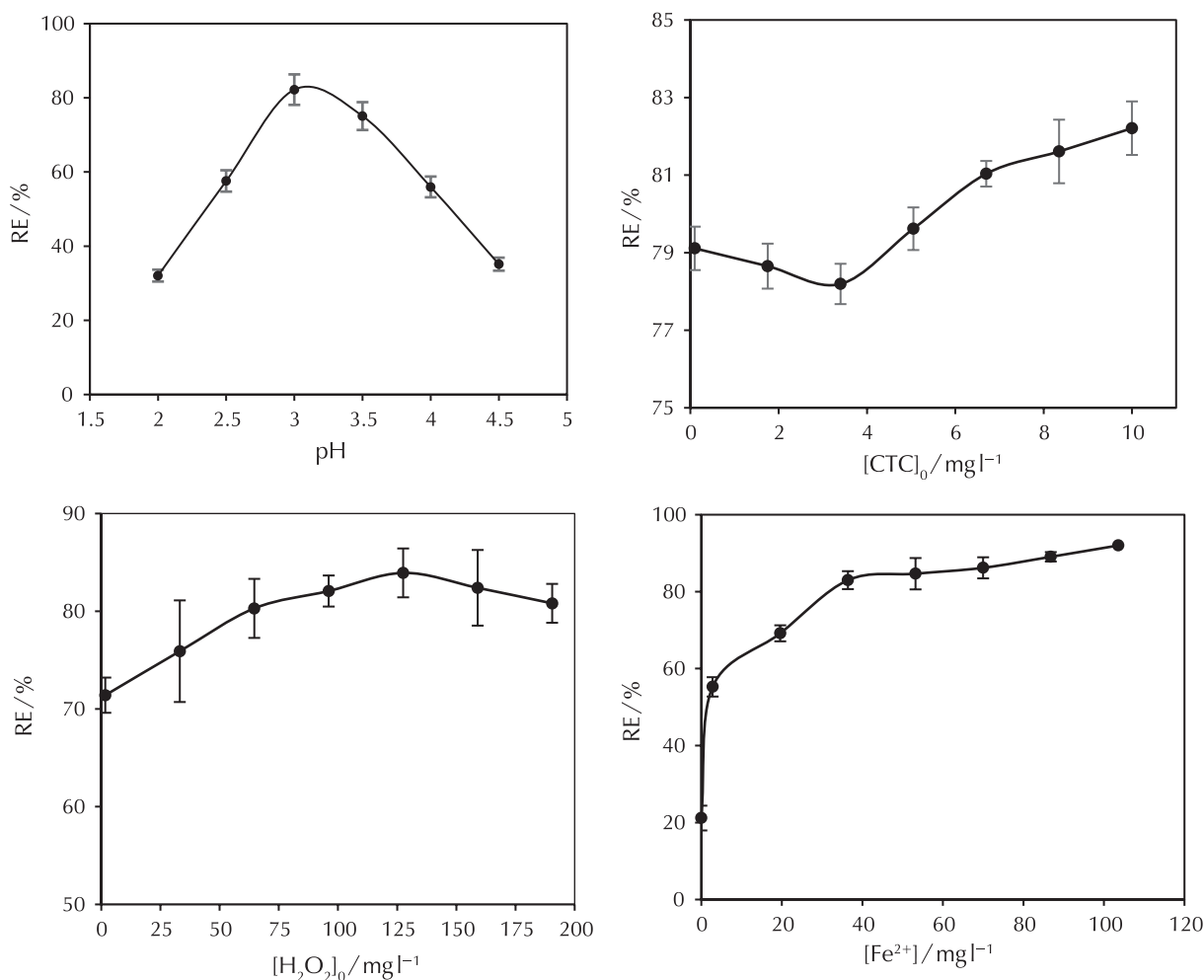
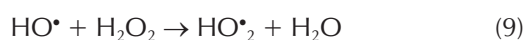


Fig. 2 – Effect of chemical parameters (pH and concentrations of CTC, H_2O_2 , and Fe^{2+}) on CTC removal by PFO. For $[CTC]_0$: pH 3, 64.627 mg l^{-1} of H_2O_2 and 36.4 mg l^{-1} of Fe^{2+} , for $[H_2O_2]_0$: pH 3, 10 mg l^{-1} of CTC and 36.4 mg l^{-1} of Fe^{2+} , and for $[Fe^{2+}]_0$: pH 3, 10 mg l^{-1} of CTC, and $127.552 \text{ mg l}^{-1}$ of H_2O_2 .

tion is due to the high concentration of hydroxyl radicals resulting in the decomposition of hydrogen peroxide molecules, which promotes the transformation of CTC molecules. Fig. 2 illustrates that also by using additional H_2O_2 above $127.552 \text{ mg l}^{-1}$, a weak stabilisation in RE occurred. This must have been due to the scavenging effect of HO^\bullet by H_2O_2 resulting in the production of perhydroxyl radicals (Eq. (9)), which are much less reactive, and do not contribute to the oxidative degradation of the organic substrate.³⁶⁻³⁸



Ferrous ions act as a catalyst at a pH below 4. Moreover, organic molecules removal is directly proportional to catalyst (Fe^{2+}) concentration. This is mainly caused by the increase in radicals concentration, which promotes the transformation efficiency of organic contaminants, such as dyes and wastewater. The hydroxyl radicals were produced more rapidly in the reaction medium because of the increase in the concentration of the catalyst.²¹ The same result was observed by Han et al., who studied the degradation of oxytetracycline and tetracycline by photo-Fenton process; the oxidation improved by increasing the concentration of ferrous ions.⁴⁰ Fig. 2 shows that removal of CTC from aqueous solution improved with catalyst dose as it reaches 80% when (Fe^{2+}) was around 36.4 mg l^{-1} . With ferrous cations overdose (increased by 67 mg l^{-1}), RE increased only by 12%, from which we consider an optimal concentration of ferrous cations of 36.4 mg l^{-1} .

However, it should be noted that these experiments were carried out for a CTC concentration of 10 mg l^{-1} , which requires high doses of iron. Thus, reducing the amount of iron in PFO requires a decrease in the amount of the polluting molecule.

Yet, the reviewed literature showed that conventional chemical (ultrasonification, Fenton oxidation, and ferro-sonification) or enzymatic treatments of CTC yielded a maximum removal of 80%.^{2,15,17,41,42}

It is important to mention that no transformation of the CTC molecules (for an account of 10 mg l^{-1}) in aqueous solutions was observed under solar irradiation, without reaching ferrous and hydrogen peroxide concentrations of 36.4 mg l^{-1} of Fe^{2+} and $127.552 \text{ mg l}^{-1}$ for H_2O_2 due to the generation of an optimal account of hydroxyl radicals responsible for degradation of CTC.

3.2 UV-visible spectra, FTIR and HPLC analysis of the CTC treated by PFO

Along with the promising results that were obtained in terms of RE, UV-visible and HPLC analysis were performed on a treated solution, while infrared spectroscopy (FTIR) was conducted on the precipitate sample, to evaluate the qualitative efficiency of the photo-Fenton oxidation by identification of CTC transformation by-products (disappearance and appearance of functional groups). Analyses were conducted on samples before and after treatment conducted under optimal conditions. According to Fig. 3-I, the UV-visible spectrum of CTC consisted of three main characteristic absorption bands. These bands are characteristic of adjacent rings (transition $\pi \rightarrow \pi^*$), whereas the visible band is attributed to long conjugated π system linked by carbonyl groups (transition $n \rightarrow \pi^*$). Regarding the treated solution spectrum, it was found that the adsorption peak at 380 nm completely disappeared after photo-Fenton treatment. This indicated that the chromophore group was transformed and associated auxochrome groups to aromatic rings, such as chloride, hydroxyl, and amino groups were destructed. In the UV region, it is clear that the intensity of the two bands (275 and 240 nm), has been significantly reduced. This was probably due to the formation of new aromatic intermediate or other products.^{15,43} Hence, OH^\bullet is involved in a non-selective reaction, leading to the breaking of functional groups and hydroxylation of the aromatic structure of CTC, resulting in smaller organic molecules.

FTIR spectra of CTC and its precipitate are presented in Fig. 3-II. The comparison of FTIR spectra between the

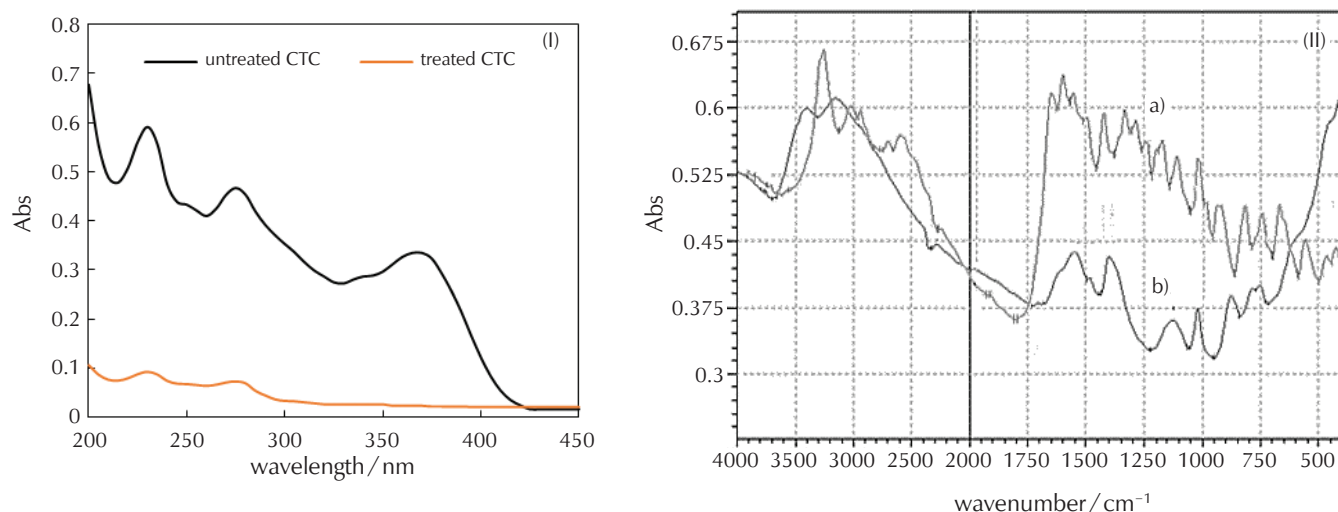


Fig. 3 – (I) UV-visible spectra of CTC before and after photo-Fenton treatment, and (II) FTIR of a) CTC, and b) its transformed products

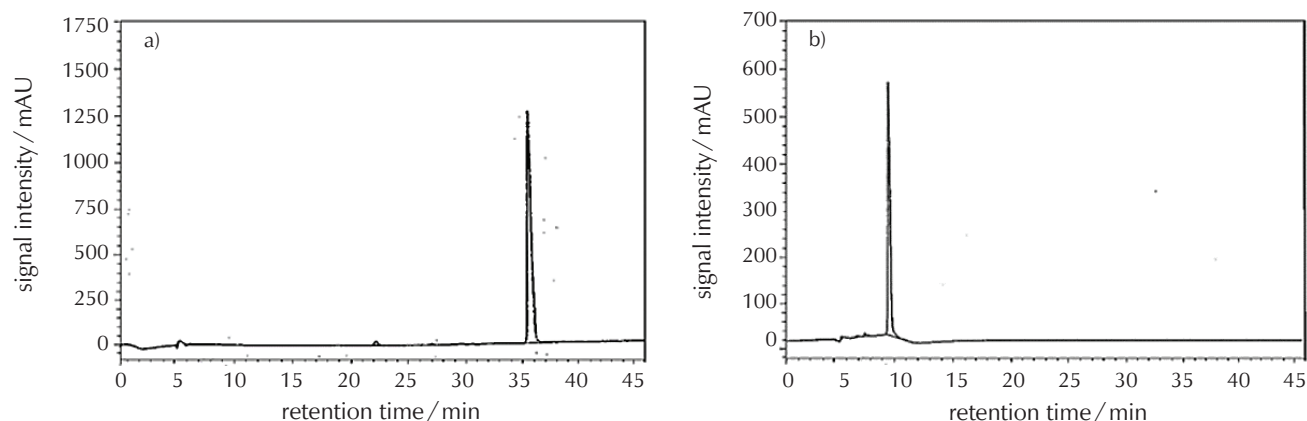


Fig. 4 – HPLC chromatograms of CTC aqueous solution (a) before photo-Fenton treatment, and (b) after photo-Fenton treatment

original sample and its metabolites indicated the transformation of the parent antibiotic molecule by PFO. Furthermore, the absorption bands in the CTC spectrum appeared at 3302.24 cm^{-1} for OH, and at 3070.78 cm^{-1} for C–H stretching vibration, as well as a stretching vibration at 1666.55 and 1620.26 cm^{-1} for $>C=O-$ of ketone and amide groups, respectively. Bands at 1581.68 and 1519.91 cm^{-1} correspond to the $-C=C-H$ in plane C–H bend characteristic of the aromatic ring. Whereas, the bands at 1442.80 cm^{-1} represented $-C-N <$ stretching vibration of the amide group. The deformation band of $-O-H$ appeared at 1357.93 cm^{-1} . The FTIR spectrum of the precipitate showed a significant change in the number and band positions compared to the CTC spectrum. The absence of the bands at 1666.55 , 1610.26 , and 1442.80 cm^{-1} stretch, suggests that the carbonyl groups may be transformed by the PFO. A new position of bands of $-C=C-$ of the aromatic ring group appeared at 1550.68 and 1620 cm^{-1} , this may be due to a bathochromic effect of new substituted groups.

HPLC chromatogram of the CTC original solution (Fig. 4-a) showed an intense peak in retention time equal to 36.34 min, and two small peaks at retention times of 6.005 and 23.232 min, corresponding to impurities contained in the original CTC sample. However, from the chromatogram of transformation by-products (Fig. 4-b), it can be seen that no peak corresponding to the CTC appeared, whereas a new peak occurs at a retention time equal to 9.117 min.

This indicates the effective transformation of some functional polar groups of CTC molecules by hydroxyl radicals, leading to the formation of new molecules. Han et al. proposed a degradation pathway mechanism of both tetracycline and oxytetracycline molecules by PFO. Firstly, the double-bond of TC (and oxytetracycline) was a susceptible site for the $HO\cdot$ attack and it was initiated at the $C_{11A}-C_{12}$ double-bond site. For the TC (similar structure to CTC), it was the dehydration of the C_6-C_{5A} product which confirmed the formation of an aldehyde group ($HC=O$). Secondly, another transformation product was formed by the dehydration of C_6-C_{5A} and demethylation⁴⁰.

However, results of the phytotoxicity test (not presented) of modal samples and their supernatant, carried out on

two kinds of seeds: *Sorghum vulgare* and *Pisum sativum* L., showed that the germination of both seeds watered with the by-product of CTC was not very different from their germination in distilled water (100 % vs. 97.47 %). Likewise, a lower percentage of germination of *S. vulgare* and *P. sativum* with lower lengths of the radicle and plumule in CTC origin solution indicated that these samples were more toxic to these plants than the metabolite products obtained from PFO.

3.3 ANN modelling

As illustrated in Fig. 5, the optimised artificial neural network (OANN) structure consists of three layers: the input layer, the hidden layer with the *tansig* transfer function, and the output layer with the linear transfer function (*purelin*). The design of an OANN model aims to determine the following elements: the MLP network type, the number of hidden neurons, the transfer function of the hidden neurons, and the number of iterations.³³

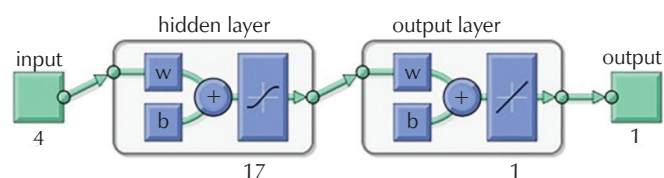


Fig. 5 – Block diagram of the model

Table 3 summarises the network topology for the optimal ANN structure predicting the removal efficiency of CTC. The number of hidden neurons was changed from 7 to 17, and the LM algorithm was applied in this work.

The OANN was found after 150 000 iterations with one hidden layer containing 17 neurons. From the results presented in Table 4, the best model was found with an RMSE value of 0.0073 and an R^2 value of 0.9983. Also, we observed that, for the RE of CTC, the MAE value compared to the data used was less than $3.3 \cdot 10^{-3}$ for the training

Table 3 – Structure of the neural network

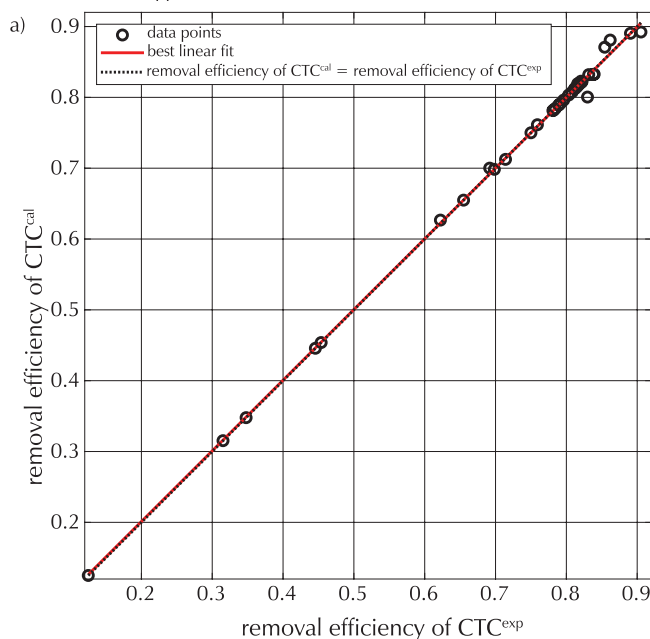
Network type	No. of neurons in hidden layer	Hidden layer transfer function	Output layer transfer function	Learning algorithm	No. of iterations
Single layer MLP	17	tansig	purelin	Levenberg-Marquardt	150000

phase, and $6.1 \cdot 10^{-3}$ for the generalisation phase. The comparison between experimental and predicted results obtained from the optimised ANN model for the training and overall data is shown schematically in Fig. 6. The determination coefficient R^2 of the linearisation curve is equal to 0.9960. We also noticed that, in this phase, the neural model perfectly reproduced the data that was used for training and validation.

Table 4 – Statistical performance of the optimised artificial neural network

Type of error	Training	Test	Validation	Overall data
MSE	$9.0764 \cdot 10^{-9}$	0.0010	$1.7008 \cdot 10^{-7}$	0.0002
RMSE	0.0073	0.0164	0.0150	0.0108
NRMSE	0.0001	0.0441	0.0006	0.0178
MAE	0.0033	0.0129	0.0108	0.0061
R^2	0.9983	0.9930	0.9804	0.9960

Best Linear Fit (App): RE of $CTC^{cal} = (1)(RE\ of\ CTC^{exp}) + (0.0015)$, $R^2 = 0.99828$



3.4 Global sensitivity analysis

The evaluation process provided a neural matrix of connection weights. The OANN weight matrix can be applied to analyse the sensitivity of the inputs to the desired output. Garson proposed an equation based on the partitioning of connection weights (Eq. (10)), where I_j is the relative sensitivity of the j^{th} input variable to the output parameter; N_i and N_h represent the number of input and hidden neurons, respectively; and W represents connection weights.⁴⁴ The exponents i, h, and o refer to the input, hidden, and output layers, respectively. Accordingly, indices k , m , and n refer to input, hidden, and output neurons, respectively.

$$I_j = \frac{\sum_{m=1}^{m=N_h} \left(\left(\frac{W_{jm}^{ih}}{\sum_{k=1}^{N_i} W_{km}^{ih}} \right) \cdot (W_{mn}^{ho}) \right)}{\sum_{k=1}^{k=N_i} \left(\sum_{m=1}^{m=N_h} \left(\frac{[W_{km}^{ih}]}{\sum_{k=1}^{N_i} W_{km}^{ih}} \right) \cdot (W_{mn}^{ho}) \right)} \quad (10)$$

The relative sensitivity of the different variables is shown in Fig. 7. As may be seen, all the variables have important effects on the removal efficiency of CTC. Therefore, it can be observed that the highest contribution was obtained by the initial concentration of Fe^{2+} (33 %), followed by the initial concentration of CTC (24 %), as well as the initial concentration of H_2O_2 (23 %), and lastly, the participation of the molecular mass (20 %).

Best Linear Fit (All): RE of $CTC^{cal} = (1)(RE\ of\ CTC^{exp}) + (-0.0042)$, $R^2 = 0.996$

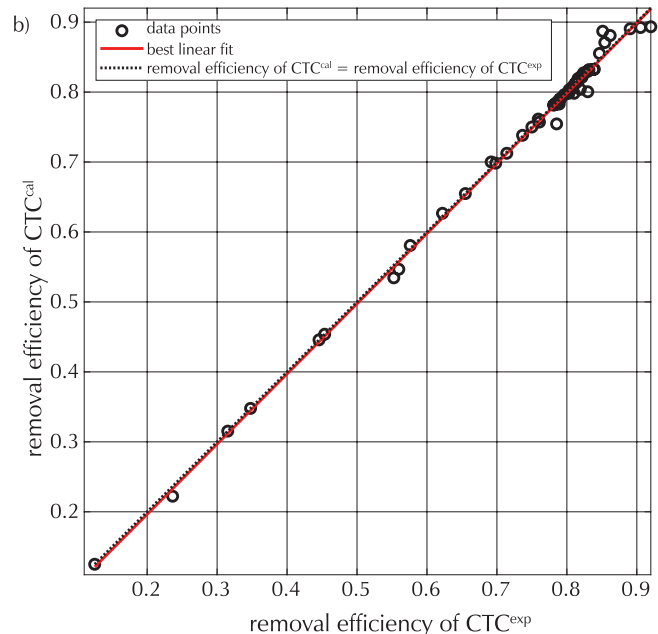


Fig. 6 – Linear regression curve of the experimental RE of CTC with the calculated RE of CTC by the ANN optimised for a) the training phase, and b) the overall phase, with topology 4 : 17 : 1

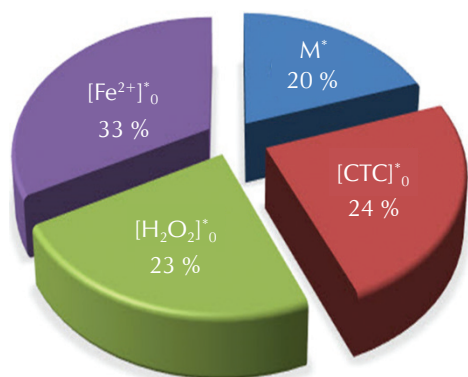


Fig. 7 – Relative importance of the input variables on the RE of CTC

3.5 Graphical user interface for predicting CTC removal efficiency

The OANN model was implemented in graphical interface designed using MATLAB software, and shown in Fig. 8. This interface can calculate the desired output knowing only the selected inputs. The programme will therefore enable a simple and fast calculation of the RE.

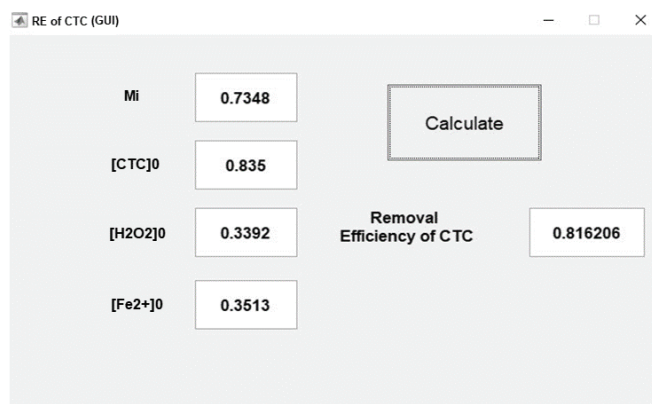


Fig. 8 – MATLAB interface for CTC removal efficiency prediction via OANN

3.6 Interpolation and extrapolation

In order to measure the robustness of the developed model for CTC removal by PFO, it was tested at two database sets, one belonging to the domain of validity (interpolation), and the other outside the domain of validity (extrapolation). Fig. 9 shows the values of statistical coefficients for 07 interpolation points. Each interpolation point is calculated by the arithmetic mean between two successive experimental values. The experimental output, (RE^{exp}), is calculated by the arithmetic mean between two successive experimental values.

As illustrated in Fig. 8, the results obtained and explored for the interpolation test are in perfect agreement with a

minimum MSE value of $6.6781 \cdot 10^{-5}$ and a high determination coefficient equal to 0.9920. Then for the extrapolation test, the MSE (compared to the experimental values) value is $9.0030 \cdot 10^{-4}$. These results showed the precision and robustness of the established ANN model of CTC removal by PFO.

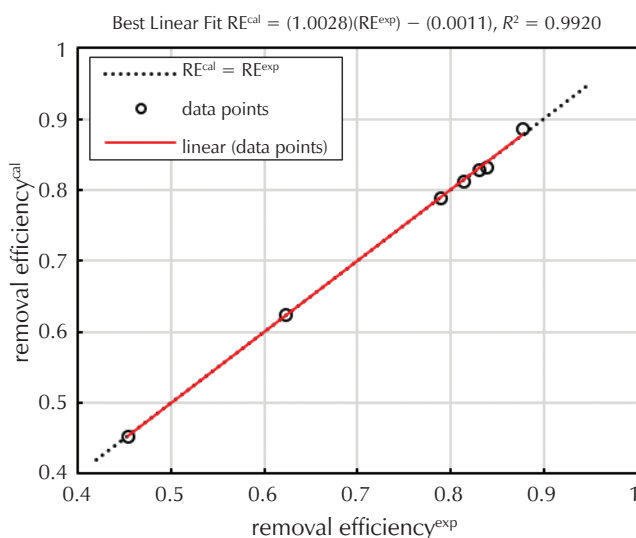


Fig. 9 – Simulation of the results of interpolation

4 Conclusion

This study aimed to determine CTC removal efficiency experimentally and by ANN modelling. The chemical oxidation by acting $\cdot OH$ on the CTC molecule showed that removal efficiency was strongly affected by pH, H_2O_2 , and Fe^{2+} doses. Photo-Fenton oxidation optimisation was then performed to investigate a maximum CTC removal efficiency; it was found to be 82.987 % at pH 3, hydrogen peroxide, ferrous ions and CTC concentrations corresponding to: $127.552 \text{ mg l}^{-1}$, 36.4 mg l^{-1} , and 10 mg l^{-1} , respectively. Analyses by UV-visible spectroscopy, FTIR spectroscopy, and HPLC confirm the transformation of some substituted groups in the polycyclic structure of the CTC molecule. The toxicity test proved that the applied photo-Fenton process was capable of degrading CTC molecules into non-toxic metabolites (results not presented).

The optimal architecture of the ANN was obtained for a topology of 4 : 17 : 1, with a *tansig* as the transfer function of the hidden layer, and the *purelin* as the transfer function in output layer. Also, the OANN model for the prediction of the RE was statistically evaluated in terms of RMSE and R^2 ; the results showed that the OANN model had a very low RMSE of 0.0108 and a high correlation coefficient of 0.9960. Based on the OANN model, a sensitivity analysis was conducted to assess the effects of the inputs on the output; the results showed that all phenomenological inputs strongly affect the removal of CTC. A user-friendly graphical user interface was designed using MATLAB software, to facilitate the use of this model.

ACKNOWLEDGEMENTS

The authors would like to thank the Director of LBMPT Laboratory for providing the help and data used in this study.

List of abbreviations and symbols

ANN	– artificial neural network
AOP	– advanced oxidation process
C_0	– initial CTC concentration, mg l^{-1}
C_t	– CTC concentration at a time t , mg l^{-1}
CTC	– chlortetracycline chlorhydrate
FTIR	– Fourier transform infrared
HPLC	– high-performance liquid chromatography
I_j	– relative sensitivity of the j^{th} input variable to the output parameter
M_i	– molecular weight of each molecule, such as chlortetracycline chlorhydrate, hydrogen peroxide, and iron
MAE	– absolute mean error
MSE	– mean square error
NRMSE	– root of the normalised mean squared error
N_i and N_h	– number of neurons in input and hidden layer, respectively
PFO	– photo-Fenton oxidation
RE	– removal efficiency, %
TC	– tetracycline
RMSE	– root mean square error
R^2	– coefficient of determination
Y_{norm}	– normalised value
y	– experimental data
y_{max}	– maximum experimental value
y_{min}	– minimum experimental value
W	– connection weights

References
Literatura

1. J. Rivera-Utrilla, M. Sánchez-Polo, M. Á. Ferro-García, C. Prados-Joya, R. Ocampo-Pérez, Pharmaceuticals as emerging contaminants and their removal from water. A review, *Chemosphere* **93** (7) (2013) 1268–1287, doi: <https://doi.org/10.1016/j.chemosphere.2013.07.059>.
2. M. Naghdi, M. Taheran, S. K. Brar, A. Kermanshahi-pour, M. Verma, R. Y. Surampalli, Removal of pharmaceutical compounds in water and wastewater using fungal oxidoreductase enzymes, *Environ. Pollut.* **234** (2018) 190–213, doi: <https://doi.org/10.1016/j.envpol.2017.11.060>.
3. L. F. Stadlmair, T. Letzel, J. E. Drewes, J. Grassmann, Enzymes in removal of pharmaceuticals from wastewater: A critical review of challenges, applications and screening methods for their selection, *Chemosphere* **205** (2018) 649–661, doi: <https://doi.org/10.1016/j.chemosphere.2018.04.142>.
4. M. Bilal, S. S. Ashraf, D. Barceló, H. M. N. Iqbal, Biocatalytic degradation/redefining “removal” fate of pharmaceutical active compounds and antibiotics in the aquatic environment, *Sci. Total Environ.* **691** (2019) 1190–1211, doi: <https://doi.org/10.1016/j.scitotenv.2019.07.224>.
5. X. Wen, Y. Jia, J. Li, Degradation of tetracycline and oxytetracycline by crude lignin peroxidase prepared from *Phanerochaete chrysosporium* – a white rot fungus, *Chemosphere* **75** (8) (2009) 1003–1007, doi: <https://doi.org/10.1016/j.chemosphere.2009.01.052>.
6. O. F. S. Khasawneh, P. Palaniandy, Occurrence and removal of pharmaceuticals in wastewater treatment plants, *Process Saf. Environ. Prot.* **150** (2021) 532–556, doi: <https://doi.org/10.1016/j.psep.2021.04.045>.
7. P. R. Rout, T. C. Zhang, P. Bhunia, R. Y. Surampalli, Treatment technologies for emerging contaminants in wastewater treatment plants: A review, *Sci. Total Environ.* **753** (2021) 141990, doi: <https://doi.org/10.1016/j.scitotenv.2020.141990>.
8. T. Rasheed, M. Bilal, F. Nabeel, M. Adeel, H. M. N. Iqbal, Environmentally-related contaminants of high concern: Potential sources and analytical modalities for detection, quantification, and treatment, *Environ. Int.* **122** (2019) 52–66, doi: <https://doi.org/10.1016/j.envint.2018.11.038>.
9. R. Antón-Herrero, C. García-Delgado, M. Alonso-Izquierdo, G. García-Rodríguez, J. Cuevas, E. Eymar, Comparative adsorption of tetracyclines on biochars and stevensite: Looking for the most effective adsorbent, *Appl. Clay Sci.* **160** (2018) 162–172, doi: <https://doi.org/10.1016/j.clay.2017.12.023>.
10. D. Xu, Y. Gao, Z. Lin, W. Gao, H. Zhang, K. Karnowo, X. Hu, H. Sun, S. S. A. Syed-Hassan, S. Zhang, Application of Biochar Derived From Pyrolysis of Waste Fiberboard on Tetracycline Adsorption in Aqueous Solution, *Front. Chem.* **7** (2020) 943, doi: <https://doi.org/10.3389/fchem.2019.00943>.
11. Z. Song, Y. L. Ma, C. E. Li, The residual tetracycline in pharmaceutical wastewater was effectively removed by using MnO_2 /graphene nanocomposite, *Sci. Total Environ.* **651** (2019) 580–590, doi: <https://doi.org/10.1016/j.scitotenv.2018.09.240>.
12. J. Scaria, K. V. Anupama, P. V. Nidheesh, Tetracyclines in the environment: An overview on the occurrence, fate, toxicity, detection, removal methods, and sludge management, *Sci. Total Environ.* **771** (2021) 145291, doi: <https://doi.org/10.1016/j.scitotenv.2021.145291>.
13. M. S. Gaballah, J. Guo, H. Sun, D. Aboagye, M. Sobhi, A. Muhmood, R. Dong, A review targeting veterinary antibiotics removal from livestock manure management systems and future outlook, *Bioresour. Technol.* **333** (2021) 125069, doi: <https://doi.org/10.1016/j.biortech.2021.125069>.
14. R. Puicharla, D. P. Mohapatra, S. K. Brar, P. Drogui, S. Auger, R. Y. Surampalli, Degradation of chlortetracycline in wastewater sludge by ultrasonication, Fenton oxidation, and ferro-sonication, *J. Environ. Chem. Eng.* **2** (3) (2014) 1596–1603, doi: <https://doi.org/10.1016/j.jece.2014.06.001>.
15. R. Pulicharla, S. K. Brar, T. Rouissi, S. Auger, P. Drogui, M. Verma, R. Y. Surampalli, Degradation of chlortetracycline in wastewater sludge by ultrasonication, Fenton oxidation, and ferro-sonication, *Ultrason. Sonochem.* **34** (2017) 332–342, doi: <https://doi.org/10.1016/j.ultsonch.2016.05.042>.
16. B. Halling-Sørensen, A. M. Jacobsen, J. Jensen, G. Sengeløv, E. Vaclavik, F. Ingerslev, Dissipation and effects of chlortetracycline and tylosin in two agricultural soils: A field-scale study in southern Denmark, *Environ. Toxicol. Chem.* **24**(4) (2005) 802–810, doi: <https://doi.org/10.1897/03-576.1>.
17. R. Pulicharla, R. K. Das, S. Kaur Brar, P. Drogui, R. Y. Surampalli, Degradation kinetics of chlortetracycline in wastewater using ultrasonication assisted laccase, *Chem. Eng. J.* **347** (2018) 828–835, doi: <https://doi.org/10.1016/j.cej.2018.04.162>.
18. Y. Liu, Y. Gao, B. Yao, D. Zou, Removal of chlortetracycline by nano- micro-electrolysis materials: Application and mech-

- anism, *Chemosphere* **238** (2020) 124543, doi: <https://doi.org/10.1016/j.chemosphere.2019.124543>.
19. K. J. Choi, H. J. Son, S. H. Kim, Ionic treatment for removal of sulfonamide and tetracycline classes of antibiotic, *Sci. Total Environ.* **387** (1-3) (2007) 247–256, doi: <https://doi.org/10.1016/j.scitotenv.2007.07.024>.
 20. L. Lan, X. Kong, H. Sun, C. Li, D. Liu, High removal efficiency of antibiotic resistance genes in swine wastewater via nanofiltration and reverse osmosis processes, *J. Environ. Manage.* **231** (2019) 439–445, doi: <https://doi.org/10.1016/j.jenvman.2018.10.073>.
 21. N. Boucherit, M. Abouseoud, L. Adour, Direct yellow degradation by combined Fenton-enzymatic process, *Nov. Biotechnol. Chim.* **17** (2) (2018) 160–171, doi: <https://doi.org/10.2478/nbec-2018-0017>.
 22. Y. Mesellem, A. A. El Hadj, M. Laidi, S. Hanini, M. Hentabli, Computational intelligence techniques for modeling of dynamic adsorption of organic pollutants on activated carbon, *Neural Comput. Appl.* **33** (2021) 12493–12512, doi: <https://doi.org/10.1007/s00521-021-05890-2>.
 23. S. Keskes, M. Hentabli, M. Laidi, S. Hanini, Modelling Drying Time of Candésartan Cilexetil Powder Using Computational Intelligence Technique, *Kem. Ind.* **70** (3-4) (2021) 137–144, doi: <https://doi.org/10.15255/kui.2020.048>.
 24. S. Rezazi, S. Hanini, C. Si-Moussa, S. Abdelmalek, Kinetic modeling and parameters identification based on meta-heuristic optimization techniques for extraction process of *Marrubium vulgare* L. essential oil, *J. Agric. Sci. Technol.* **19** (2) (2017) 307–322.
 25. Y. Ammi, L. Khaouane, S. Hanini, Modeling and optimization of small-scale NF/RO seawater desalination using the artificial neural network (ANN), *Neural Comput. Appl.* **33** (2021) 12429–12444, doi: <https://doi.org/10.1007/s00521-021-05876-0>.
 26. M. Hamadache, C. Si-Moussa, M. Laidi, S. Hanini, S. Belmadani, Artificial Neural Network Models for Prediction of Density and Kinematic Viscosity of Different Systems of Biofuels and Their Blends with Diesel Fuel. Comparative Analysis, *Kem. Ind.* **69** (7-8) (2020) 355–364, doi: <https://doi.org/10.15255/kui.2019.053>.
 27. A. Ibrir, Y. Kerchich, N. Hadidi, H. Merabet, M. Hentabli, Prediction of the concentrations of PM1, PM2.5, PM4, and PM10 by using the hybrid dragonfly-SVM algorithm, *Air Qual. Atmos. Heal.* **14** (3) (2021) 313–323, doi: <https://doi.org/10.1007/s11869-020-00936-1>.
 28. A. Rezrazi, S. Hanini, M. Laidi, An optimisation methodology of artificial neural network models for predicting solar radiation: a case study, *Theor. Appl. Climatol.* **123** (3-4) (2016) 769–783, doi: <https://doi.org/10.1007/s00704-015-1398-x>.
 29. M. Hanini, S. Khebbache, L. Bouillaut, M. Hadji, Dynamic and adaptive grouping maintenance strategies: New scalable optimization algorithms, *Proc. Inst. Mech. Eng. Part O J. Risk Reliab.* **236** (2021) 647–660, doi: <https://doi.org/10.1177/1748006X211049924>.
 30. M. Roubehie Fissa, Y. Lahiouel, L. Khaouane, S. Hanini, QSPR estimation models of normal boiling point and relative liquid density of pure hydrocarbons using MLR and MLP-ANN methods, *J. Mol. Graph. Model.* **87** (2019) 109–120, doi: <https://doi.org/10.1016/j.jmgm.2018.11.013>.
 31. C. Si-Moussa, S. Hanini, R. Derriche, M. Bouhedda, A. Bouzidi, Prediction of high-pressure vapor liquid equilibrium of six binary systems, carbon dioxide with six esters, using an artificial neural network model, *Brazilian J. Chem. Eng.* **25** (1) (2008) 183–199, doi: <https://doi.org/10.1590/S0104-66322008000100019>.
 32. E. S. Elmolla, M. Chaudhuri, M. M. Eltoukhy, The use of artificial neural network (ANN) for modeling of COD removal from antibiotic aqueous solution by the Fenton process, *J. Hazard. Mater.* **179** (1-3) (2010) 127–134, doi: <https://doi.org/10.1016/j.jhazmat.2010.02.068>.
 33. A. El Bey, M. Laidi, A. Yettou, S. Hanini, A. Ibrir, M. Hentabli, H. Ouldkaoua, Practical Artificial Neural Network Tool for Predicting the Competitive Adsorption of Dyes on Gemini Polymeric Nanoarchitecture, *Kem. Ind.* **70** (9-10) (2021) 481–488, doi: <https://doi.org/10.15255/kui.2020.069>.
 34. E. Neyens, J. Baeyens, A review of classic Fenton's peroxidation as an advanced oxidation technique, *J. Hazard. Mater.* **98** (1-3) (2003) 33–50, doi: [https://doi.org/10.1016/S0304-3894\(02\)00282-0](https://doi.org/10.1016/S0304-3894(02)00282-0).
 35. A. Babuponnusami, K. Muthukumar, A review on Fenton and improvements to the Fenton process for wastewater treatment, *J. Environ. Chem. Eng.* **2** (1) (2014) 557–572, doi: <https://doi.org/10.1016/j.jece.2013.10.011>.
 36. P. V. Nidheesh, R. Gandhimathi, S. T. Ramesh, Degradation of dyes from aqueous solution by Fenton processes: A review, *Environ. Sci. Pollut. Res.* **20** (4) (2013) 2099–2132, doi: <https://doi.org/10.1007/s11356-012-1385-z>.
 37. L. M. Nieto, G. Hodaifa, S. Rodríguez, J. A. Giménez, J. Ochando, Degradation of organic matter in olive-oil mill wastewater through homogeneous Fenton-like reaction, *Chem. Eng. J.* **173** (2) (2011) 503–510, doi: <https://doi.org/10.1016/j.cej.2011.08.022>.
 38. M. hui Zhang, H. Dong, L. Zhao, D. Wang Xi, D. Meng, A review on Fenton process for organic wastewater treatment based on optimization perspective, *Sci. Total Environ.* **670** (2019) 110–121, doi: <https://doi.org/10.1016/j.scitotenv.2019.03.180>.
 39. S. Meriç, D. Kaptan, T. Ölmez, Color and COD removal from wastewater containing Reactive Black 5 using Fenton's oxidation process, *Chemosphere* **54**(3) (2004) 435–441, doi: <https://doi.org/10.1016/j.chemosphere.2003.08.010>.
 40. C. H. Han, H. D. Park, S. B. Kim, V. Yargeau, J. W. Choi, S. H. Lee, J. A. Park, Oxidation of tetracycline and oxytetracycline for the photo-Fenton process: Their transformation products and toxicity assessment, *Wat. Res.* **172** (2020) 115514, doi: <https://doi.org/10.1016/j.watres.2020.115514>.
 41. X. Liao, R. Zou, B. Li, T. Tong, S. Xie, B. Yuan, Biodegradation of chlortetracycline by acclimated microbiota, *Process Saf. Environ. Prot.* **109** (2017) 11–17, doi: <https://doi.org/10.1016/j.psep.2017.03.015>.
 42. V. Homem, L. Santos, Degradation and removal methods of antibiotics from aqueous matrices – A review, *J. Environ. Manage.* **92** (10) (2011) 2304–2347, doi: <https://doi.org/10.1016/j.jenvman.2011.05.023>.
 43. W. Hailei, L. Ping, P. Min, Z. Zhijun, Y. Guangli, L. Guosheng, Y. Jianming, Rapid decolorization of azo dyes by a new isolated higher manganese peroxidase producer: *Phanerochaete* sp. HSD, *Biochem. Eng. J.* **46** (3) 2009 327–333, doi: <https://doi.org/10.1016/j.bej.2009.06.008>.
 44. M. Laidi, S. Hanini, Optimal solar COP prediction of a solar-assisted adsorption refrigeration system working with activated carbon/methanol as working pairs using direct and inverse artificial neural network, *Int. J. Refrig.* **36** (1) (2013) 247–257, doi: <https://doi.org/10.1016/j.iijrefrig.2012.09.016>.

SAŽETAK

Uklanjanje klortetraciklin klorhidrata foto-Fentonovim postupkom: eksperimentalna studija i ANN modeliranje

Nabila Boucherit,^a Salah Hanini,^a Abdellah Ibrir,^b Maamar Laidi^{a,} i Mohamed Roubehie-Fissa^a*

Cilj ovog rada bio je ispitati razgradnju klortetraciklin klorhidrata (CTC) u vodenoj otopini foto-Fentonovim procesom, kao i modelirati ponašanje sustava primjenom umjetnih neuronskih mreža. Učinkovitost uklanjanja CTC-a foto-Fentonovim procesom ispitana je pod sunčevom svjetlošću. Proučavani su različiti parametri poput pH (3 do 5) te početnih koncentracija CTC-a (0,1 do 10 mg l⁻¹), vodikova peroksida (1,701 do 190,478 mg l⁻¹) i željeznih iona (2,8 do 103,6 mg l⁻¹). Dobivena je učinkovitost uklanjanja od 92 % pri pH 3, uz 10 mg l⁻¹ CTC, 127,552 mg l⁻¹ H₂O₂ i 36,4 mg l⁻¹ Fe²⁺. Koncentracija CTC-a praćena je spektrofotometrijski i tekućinskom kromatografijom, te su utvrđene neznatne koncentracije CTC-a u vodenoj otopini nakon obrade. Umjetna neuronska mreža višeslojni perceptron razvijena je za predviđanje eksperimentalne učinkovitosti uklanjanja CTC-a na temelju četiri bezdimenzionalna ulaza: molekulske mase, te početnih koncentracija CTC-a, vodikova peroksida i željeznih iona. Pronađena je najbolja mreža s visokim koeficijentom determinacije od 0,9960 i vrlo prihvatljivom srednjom kvadratnom pogreškom od 0,0108. Globalna analiza osjetljivosti potvrdila je da je najutjecajniji parametar kod uklanjanja CTC-a foto-Fentonovim procesom početna koncentracija kationa željeza s relativnom važnošću od 33 %.

Ključne riječi

Umjetne neuronske mreže, višeslojni perceptron, klortetraciklin klorhidrat, modeliranje, foto-oksidacija

^a *Biomaterials and Transport Phenomena Laboratory (LBMP), Yahia Fares University, Médéa, Alžir*

^b *Materials and Environment Laboratory (LME), Faculty of Technology, Yahia Fares University, Médéa, Alžir*

Izvorni znanstveni rad
Prispjelo 14. siječnja 2023.
Prihvaćeno 4. lipnja 2023.